Journal Name

Dynamic Article Links ►

Cite this: DOI: 10.1039/c0xx00000x

www.rsc.org/xxxxxx

ARTICLE TYPE

Role of Negatively Charged Au State in Aerobic Oxidation of Alcohols over Hydrotalcite Supported AuPd Nanoclusters

Shun Nishimura,[a] Yusuke Yakita,[a] Madoka Katayama,[b] Koichi Higashimine[b] and Kohki Ebitani[a]

Received (in XXX, XXX) Xth XXXXXXXXX 20XX, Accepted Xth XXXXXXXXX 20XX

DOI: 10.1039/b000000x

The PVP-protected bimetallic gold/palladium nanoclusters (Au_xPd_y-PVP NCs) were prepared onto the solid base hydrotalcite (HT) with various Au:Pd (*x*:*y*) molar ratios. Transmission electron microscopy showed narrow particle size distributions of Au_xPd_y-PVP NCs with a mean diameter in the range of 2.6-3.0 nm regardless of Pd contents. Aerobic oxidations of 1-phenylethanol over the Au_xPd_y-PVP/HT catalysts exhibited that their catalytic activities were significantly affected by the Pd contents. Correlations between charge transfer between Au and Pd and catalytic activity of the Au_xPd_y-PVP/HT catalyst were investigated with X-ray photoelectron spectroscopy (XPS), X-ray absorption near-edge structure (XANES), Michaelis-Menten kinetic studies for alcohol oxidation, and other analytical techniques. The peaks of Au 4*f* in the XPS spectra were shifted to lower energy side with increase of Pd contents, indicating the electron transfer from Pd to Au atoms according to the Pauling's electronegativity protocol. The electron densities in Au 5*d* orbital in the Au_xPd_y-PVP/HT catalysts estimated by the Au L_3-XANES spectra correlated well with their catalytic activities. Moreover, the kinetic studies also proposed that the electron rich Au 5*d* states, resulted from the intermetallic electron transfer from Pd atoms, strongly contributed to the rate-determination step in the alcohol oxidation. It was concluded that the electronic negativity in the Au 5*d* states controlled by the Pd contents accelerated the rate-determination step in alcohol oxidation through highly active radical-like intermediates.

Introduction

Bimetallic nanoparticeles (NPs) have attracted great interests and potentials in advanced materials science because they achieved unique performances different from those of monometallic NPs.[1] Since the catalytic activities of nano-sized Au particles were reported by Haruta in 1980s,[2,3] it makes breakthroughs in series of Au and incorporated second element NPs as catalysts such as Au cluster, AuPd, AuPt, AuAg and so on.[4-8] However, the contribution of these advanced catalysts on the reaction kinetics over the bimetallic catalyst is still questionable. In general, (i) the each element promotes different elementary reaction steps (bifunction effect), (ii) the electron transfer among two elements improve reactivity (ligand effect), and (iii) the specific group of surface atoms developed by geometric growth (ensemble effect), were considered as driving forces for significant performances of heterometallic assemblies.[9-11] The difficulties in the synthesis of uniform bimetallic NPs with various mixing ratio and/or morphologies become a barrier to discuss and compare their performances in the reaction mechanism.

From the viewpoint of energy and environmental issues, aerobic oxidation of alcohols for the synthesis of fine chemicals over a highly active heterogeneous catalyst has been investigated.[12-18] It leads to environmentally-friendly synthesis routes comparing to the stoichiometric oxidations over transition metal complexes. Additionally, the traditional process produces a large amount of undesirable salts and needs energy for separation of the product from reaction mixture. Therefore, the notable protocols for the active sites synthesis on a nanoscale has a great impact for development of highly functionalized heterogeneous catalyst in next advantage. In this regard, supported polymer capped highly dispersed bimetallic NPs catalysts, *ex.* Au@Pd-PVA/TiO_2,[19] AuPt-PVA/MgO,[20] and AuPd-PVA/C[21,22] have been extensively studied for alcohols oxidation into carbonyl compounds.

Herein, we examined the aerobic oxidation over the PVP-protected AuPd bimetallic (Au_xPd_y-PVP) NCs deposited onto the hydrotalcite (HT) catalysts with similar size distributions of Au_xPd_y-PVP NCs. The AuPd NPs are well-known as one of the most attractive active site for the catalyst for various reactions such as not only alcohol oxidation,[19-24] but also hydrogenation of 1,3-cyclooctadiene,[25,26] the direct synthesis of H_2O_2,[27-29] acetoxylation of ethylene,[30] and oxygen reduction in electrode.[31,32] The HT has been known as an effective support for various reactions such as deoxygenation, chemoselective reduction, and oxidation reactions because it exhibits turnable surface base sites on the HT, achieving highly catalytic performance through proton abstraction and uniform depositions of active metal on the surface.[33-39] It is supposed that the combination with AuPd NCs and HT become a significant heterogeneous catalyst for the alcohol oxidation. In addition, both

the careful synthesis of bimetallic NCs and study on their reaction mechanism may give the clarification of their novelties in the reaction.

Effect of the doping hetero atoms to Au nanocluster (NC) for catalytic activities has been widely focused on by several researchers.[40-42] Notably, Toshima *et al.* reported that the degree of electron transfer in the bimetallic core/shell NCs is proportional to the visible-light-induced hydrogen generation from water in the system of EDTA/$[Ru(bpy)_3]^{2+}$/MV^{2+}/metal NC. They clarified that the bimetallic NC can accept electrons more easily than the monometallic one, and which accelerated the rate-determining step; production of methyl viologen cation radical.[40] They also suggested that differences of the ionic potential between Pd and Pt could provide an uneven distribution of electrons, and the formed positive Pd shell in the Pt@Pd-PVP NCs favored the C=C double bond of diene substrate and provided good catalytic activity.[41] It has been said that the intermetallic electron transfer in the bimetallic NCs seem to play an important role in the acceleration of rate-determination step.[9,43-45]

In this study, we succeeded in the synthesis of extremely active $Au_{60}Pd_{40}$-PVP/HT possessing the highest turnover number (= 395,700) for aerobic oxidation of 1-phenylethanol (250 mmol). Thereafter, transmission electron microscopy, X-ray photoelectron spectroscopy, X-ray absorption spectroscopy, Michaelis-Menten kinetic studies for alcohol oxidation and other analytical techniques were employed in order to realize the novelty of the synthesized Au_xPd_y-PVP/HTs. By taking advantages of morphological and electronic analysis of AuPd-PVP NPs with kinetic studies in aerobic oxidation of alcohols with and without radical scavenger, it was also revealed that the remarkable activity of the Au_xPd_y-PVP/HT catalyst was strongly contributed by the electron rich Au 5*d* states, since the formed negative Au species induces the active radical-like peroxo-species formation which accelerated the rate-determination step of the alcohol oxidation.

Experimental

Chemicals and Materials

Hydrogen tetrachloroaurate tetrahydrate ($HAuCl_4$•$4H_2O$), palladium chloride ($PdCl_2$), potassium chloride (KCl), ethylene glycol (EG), sodium carbonate decahydrate (Na_2CO_3•$10H_2O$) and benzyl alcohol were supplied by Wako Pure Chemical Ind., Ltd. Co. PVP (M.W. = 58,000) and Mg-Al HT (Mg/Al = 5) were purchased from Acros Organics Co. and Tomita Pharmaceutical Co., Ltd., respectively. 2,2,6,6-Tetramethylpiperidine 1-oxyl (TEMPO) and 1-phenylethanol were provided from Tokyo Chemical Ind. Co. Ltd. 2,6-Di-*tert*-butyl-*p*-cresol, naphthalene and toluene were purchased from Kanto Chem. Co. Ltd.

Synthesis of AuPd-PVP/HT catalyst

The Au_xPd_y-PVP NCs with various Pd contents were prepared by the polyol reduction method according to the previous report[46] with some modifications. Briefly, an aqueous solution (50 ml) of $PdCl_2$ (*y* mmol) including KCl (0.1 g) and $HAuCl_4$·$4H_2O$ (*x* mmol) were mixed with PVP (0.58 g) and EG (50 ml), then the obtained mixture was refluxed for 2 h. Thereafter, HT (1.0 g) was added the formed colloidal dispersion to stabilize the formed Au_xPd_y-PVP NCs onto the surface of HT with a stirring. The obtained precipitates were filtered, washed and dried in vacuum overnight. The Pd contents were varied in the range of 0 to 100, and the total amount of both metals in the mixed solution ($x + y$) was kept as 0.1 mmol; *i.e.* the prepared Au_xPd_y-PVP/HT catalyst contains 0.1 mmol metal per g in stoichiometry.

Aerobic Oxidation of Alcohols

All reactants and solvent were purified before use. Oxidations were carried out in the glass tube attached with a reflux condenser. In general procedure, 2 mmol of alcohol in 5 ml of toluene and the Au_xPd_y-PVP/HT catalyst were added to the glass tube, and purged with an O_2 flow before reaction under stirring (500 rpm). Subsequently, the mixture was stirred at desired temperature for a given time under an O_2 flow (20 ml•min^{-1}) in atmospheric pressure. After the reaction, resultant solution was filtered off the solid catalyst using Millex syringe filter (0.20 μm). The products were analyzed by GC equipped with a DB-FFAP (30 m length, 0.25 mm i.d.) or a DB-1 (30 m length, 0.25 mm i.d.) column with FID detector using the internal standard curve method. The naphthalene was used as an internal standard to determine the conversion and yield.

Characterizations

Transmission electron microscopy (TEM) was taken by Hitachi H-7650 at 100 kV. An energy-dispersive X-ray analysis (EDS) attached to the scanning TEM-high angle annular dark field (STEM-HAADF) was performed with JEOL JEM-ARM200F at 200 kV. Ultraviolet and visible (Uv-vis) spectra were measured by Perkin-Elmer Lambda35 spectrometer at room temperature with light path length of 1 cm. X-ray photoelectron spectroscopy (XPS) was measured on Shimadzu·Kratos AXIS-ULTRA DLD spectrometer using Al target at 15 kV and 10 mA. The binding energies were calibrated with the C 1*s* level (284.8 eV) as the internal standard reference. Induced couple plasma spectroscopy (ICP) was recorded with Shimadzu ICPS-7000 Ver.2. The contents of Pd and Au on the catalyst were estimated by the standard curve method. X-ray absorption near edge structure (XANES) measurement was performed at the BL01B1 in SPring-8 of Japan Synchrotron Radiation Research Institute (JASRI). The Au L_3-edge XANES spectra was recorded at room temperature using a Si(111) monochromator.

Results and Discussion

Aerobic oxidations of 1-phenylethanol to acetophenone were carried out with Au_xPd_y-PVP/HTs with various Pd contents. The results are summarized in Table 1. Size distributions of the Au_xPd_y-PVP/HTs were also listed in the Table 1, and these values were similar among Au_xPd_y-PVP/HTs except for Au_{100}-PVP/HT (aggregation) (See electronic supporting information (ESI), Figure S1). The Au_{100}-PVP/HT showed no activity (entry 1). The bimetallic Au_xPd_y-PVP/HTs exhibited difference activities, and the $Au_{60}Pd_{40}$-PVP/HT achieved the most significant activity among Au_xPd_y-PVP/HTs (entries 2-5). The excellent yields of the $Au_{60}Pd_{40}$-PVP/HT were also performed even at 300 K (>99% yield, entry 3^h) and under air condition (>99 yield, entry 3^i). It is likely that the Pd contents in the Au_xPd_y-PVP/HTs have a strong influence on catalytic activity for aerobic oxidation of 1-phenylethanol. We also

Table 1 Aerobic oxidation of 1-phenylethanol under base free conditions using Au_xPd_y-PVP/HT catalysts with various Pd contents.[a]

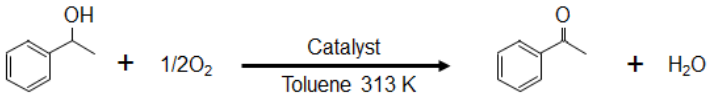

Entry	Catalyst[b]	Conv. (%)[c]	Yield. (%)[c]	Particle size (nm)[d]	Metal amount (mmol·g^{-1})[e]	
					Au	Pd
1	Au_{100}-PVP/HT	2	0	Agglomerate	0.075	0
2	$Au_{80}Pd_{20}$-PVP/HT	100, 92[g]	99, 92[g]	3.1	0.115	0.034
3	$Au_{60}Pd_{40}$-PVP/HT	100, 100,[g] 100,[h] 100[i]	>99, >99,[g] >99,[h] >99[i]	2.6	0.054	0.042
4	$Au_{40}Pd_{60}$-PVP/HT	58	57	2.6	0.052	0.098
5	$Au_{20}Pd_{80}$-PVP/HT	19	19	2.6	0.023	0.135
6	Pd_{100}-PVP/HT	2	0	2.6	0	0.154
7	Au_{100}/HT[f]	18	18	2.6	0.075	0

[a]Reaction conditions: 1-phenylethanol (2 mmol), catalyst (0.2 g; Au＋Pd = 0.02 mmol), mole ratio of alcohol / (Au+Pd) = 100 , toluene (5 ml), 313 K, 1 h, O_2 flow (20 ml•min^{-1}). [c]Analyzed by GC using an internal standard technique. [d]Determined by TEM measurement about 500 NPs for each sample. [e]Estimated with ICP analysis. [f]Reduced by KBH_4. [g]1-phenylethanol (4 mmol). [h]300 K, 3 h. [i]Air purge, 12 h.

tested its reusability in aerobic oxidation of 1-phenylethanol, then it could be reused without significant loss of activity and selectivity after washing with acetone followed by a 10 wt% Na_2CO_3 aqueous solution and drying in vacuum (Figure S2). The reaction over the Pd_{100}-PVP/HT catalyst was rarely proceeded regardless of the small particle size (2.6 nm) whereas the bare Au NPs stabilized on HT (Au_{100}/HT) catalyst with a similar size distribution (2.6 nm) and metal amount (0.075 Au mmol•g^{-1}) showed little activity (entry 7). It is supposed that the Au atoms in Au_xPd_y-PVP NPs mainly play as an active site for the alcohol oxidation. Furthermore, scope for the $Au_{60}Pd_{40}$-PVP/HT in aerobic oxidation of various alcohols to the corresponding aldehydes or ketones under mild reaction condition was also examined. Though the presence of substituents such as *p*-H_3CO- and *p*-Cl- on the aromatic ring affect the yield of the product (*vide infra*), the $Au_{60}Pd_{40}$-PVP/HT catalyst allows adaptive oxidation for various alcohol substrates (Table S1).

The turnover number (TON) and turnover frequency (TOF) of the oxidation of 1-phenylethanol (250 mmol) into acetophenone were at up to 395,700 and 69,100 h^{-1}, respectively, at 423 K for 24 h in the absence of solvents with 35 % yield and 95 % selectivity.[47,48] These values are comparable to the previous reports (detailed information is listed in Table S2); *i.e.* Au/HT (93% yield, TON = 200,000, TOF = 8,300 h^{-1}),[36] Au/CeO_2 (TON = 250,000 (after three recycles), TOF = 12,500 h^{-1}),[12,13] PdHAP (37.8% yield, TON = 236,000, TOF = 9,800 h^{-1}),[49] and Au@Pd/TiO_2 (TOF = 269,000 h^{-1}).[19] These results clearly show that the present $Au_{60}Pd_{40}$-PVP/HT is excellent catalyst for oxidation of alcohol. Investigation of different supports with $Au_{60}Pd_{40}$-PVP NCs also provided the novelty of the combination of AuPd bimetallic NCs and HT as a catalyst for alcohol oxidation reaction (Table S3).

To clarify the reaction pathway over the $Au_{60}Pd_{40}$-PVP/HT, investigations using radical scavenger were performed. As the results shown in Figure 1, the TEMPO moderately influenced the oxidation rate of 1-phenylethanol. It has been reported that the alcohol oxidation over the monometallic metal supported catalysts proceed the metal-alcohoxide formation mechanism and which is not affected by the radical scavengers.[16-18,37,49] Interestingly, our finding is different from the such previous studies over monometallic catalyst (*via infra*). Additionally, if the dominant reaction mechanism involving the formation of carbon-centered free radical intermediates over the Au_xPd_y-PVP/HT catalyst, the yield of acetophenon should be unchanged by such a small amount of TEMPO radical scavenger (0.0032 mmol). The 2,6-di-*tert*-butyl-*p*-cresol (0.0454 mmol) also influenced the oxidation rate of 1-phenylethanol (67% yield after 1 h reaction). These results implied that another radicalic intermediates were seemed to be formed during the reaction (*vide infra*).

From comparison of the reaction rate between primary and secondary alcohols, the oxidation of 1-phenylethanol (TOF = 755 h^{-1}) was faster than that of benzyl alcohol (TOF = 552 h^{-1}),

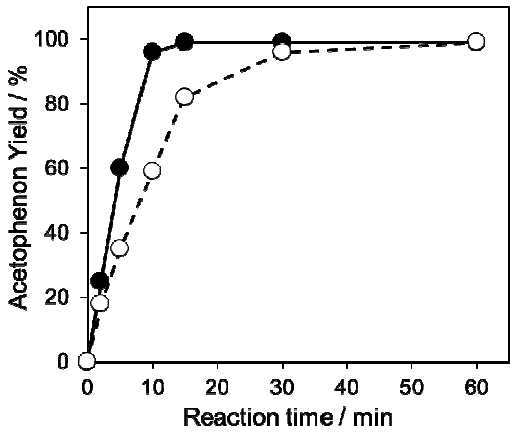

Fig. 1 Time-course of aerobic oxidation of 1-phenyl ethanol in the absence (closed circle) or presence (open circle) of TEMPO. Reaction conditions: 1-phenylethanol (2 mmol), $Au_{60}Pd_{40}$-PVP/HT catalyst (0.2 g), TEMPO (0 or 0.5 mg), toluene 5 ml, 313 K, O_2 flow (20 ml•min^{-1}).

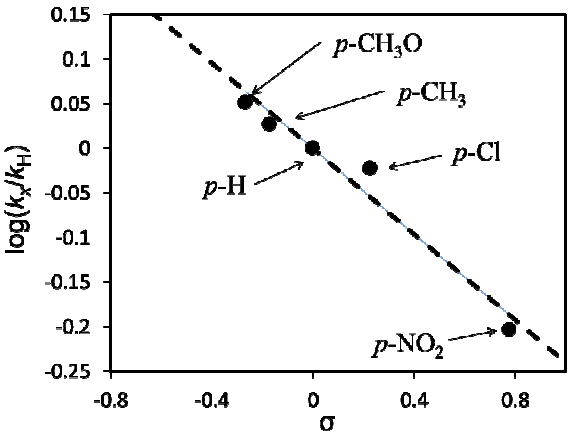

Fig. 2 Hammet plots for oxidation of benzyl alcohol and *p*-substituted benzyl alcohols. Reaction condtion: alcohol (0.5 mmol), toluene (5 ml), $Au_{60}Pd_{40}$-PVP/HT catalyst (10 mg), 313 K, 5 min, O_2 flow (20 ml•min^{-1}).

individually (Figure S3). In contrast, benzyl alcohol (TOF = 315 h^{-1}) was faster oxidized than 1-phenylethanol (TOF = 69 h^{-1}) using an equimolar mixture of alcohols (intermolecular competitive oxidations) (Figure S4). These observations were also reported, previously.[14,17] It is said that the faster oxidation of primary alcohol than secondary alcohol in competitive oxidation presumably supported the formation of metal-alcoholate intermediate species through the ligand exchange.[50-52] To determine the presence of a carbocationic character in the transition state of the reaction, the logarithm of the rate constants, $\log(k_X/k_H)$, against substituent constant (σ) reported by Hammet[53] were plotted in the aerobic oxidation of *p*-substituted benzyl alcohols. As shown in the Figure 2, there is a reasonable linearity between $\log(k_X/k_H)$ and the σ parameter in the following order of the reactivity; *p*-CH_3O > *p*-CH_3 > *p*-H > *p*-Cl > *p*-NO_2. The Hammet ρ value was –0.240 (R^2 = 0.96). The negative value indicates that a carbocationic character on the benzylic carbon is an intermediate specie in the transition state of the alcohol oxidation over the Au_xPd_y-PVP/HT catalyst. Consequently, it

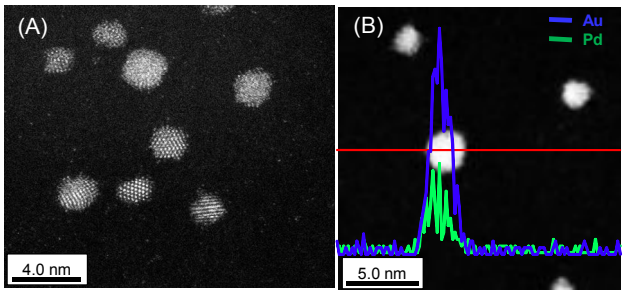

Fig. 3 (A) STEM-HAADF image and (B) STEM-EDS line analysis of the $Au_{60}Pd_{40}$-PVP NCs. The blue and green lines are corresponding to the presences of Au and Pd elements, respectively.

is likely that the oxidation of alcohols over the Au_xPd_y-PVP/HT catalyst is progressed *via* the alkoxide intermediate.

In order to understand the superiority of the $Au_{60}Pd_{40}$-PVP/HTs for alcohols oxidation, their morphologies and electronic states were also investigated. Figure 3 shows the STEM-HAADF image and STEM-EDS line analysis of the $Au_{60}Pd_{40}$-PVP NCs. Since the STEM-HAADF analysis technique offers enhanced contrast proportional to Z^2, the heavier Au atoms (atomic number; Z = 79) give rise to a brighter image than the lighter Pd atoms (Z = 46). However, the STEM-HAADF image of $Au_{60}Pd_{40}$-PVP NCs looks uniform contrast (Figure 3A). As the result of quantitative analysis of EDS profile, the $Au_{60}Pd_{40}$-PVP NCs was likely composed with homogeneous mixed 60.2% Au and 39.8% Pd atoms (Figure 3B). These values agreed well with the stoichiometric ratio in $Au_{60}Pd_{40}$ NC. Moreover, other components of Au_xPd_y-PVP NCs show similar images in the STEM-HAADF images and the STEM-EDS line analysis (Figure S5), and the later proposed that their Au/Pd ratios also suits to the stoichiometric ratio of Au/Pd for each. The detailed morphologies of Au_xPd_y-PVP NCs could not be resolved due to the extremely small size of the NCs and the difficulty in obtaining electron beam diffraction. The Uv-vis spectra of the Au_xPd_y-PVP NCs dispersed solutions show no specific surface plasmon (SPR) absorption of the Au NPs

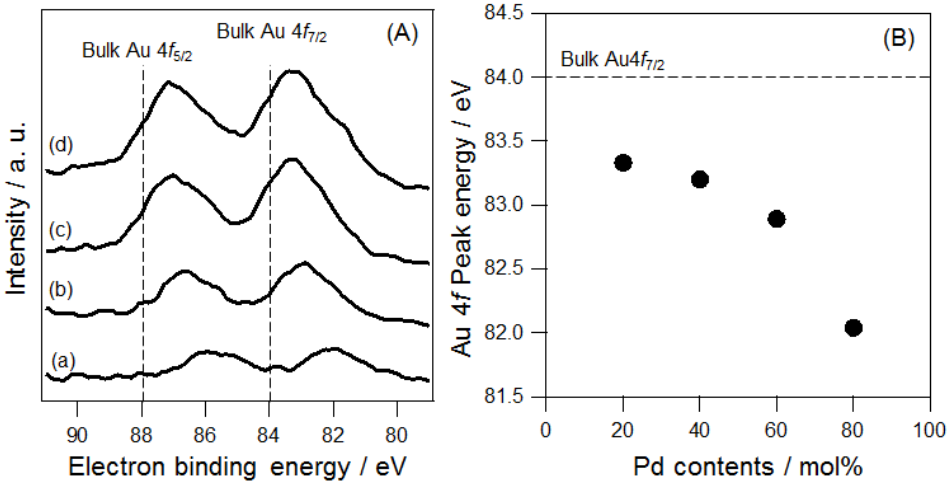

Fig. 4 (A) XPS spectra of (a) $Au_{20}Pd_{80}$-PVP, (b) $Au_{40}Pd_{60}$-PVP, (c) $Au_{60}Pd_{40}$-PVP and (d) $Au_{80}Pd_{20}$-PVP NCs around Au 4*f* components, and (B) plots of the peak positions of Au $4f_{7/2}$ as a function of Pd contents.

around 520-580 nm[54] whereas the Au_{100}-PVP NPs shows the SPR feature at 527 nm (Figure S6). As mentioned above, the unimodels and narrow size distributions among Au_xPd_y-PVP NCs in various Pd contents were observed (Figure S1). If the alloy is not formed, the size related to the isolated Au NPs will be also obtained. Therefore, distribution would lead to a broad or bimodal one due to different growth rates for the two metal NPs and the SPR phenomena. According to these results, it was suggested that the compositions of the Au_xPd_y-PVP NCs were different from that of Au or Pd mother clusters and the mixtures of isolated Au and Pd NCs, which indicates that each particle contains both Au and Pd elements in the form of alloy phase. It seems to be possible to form the alloy *via* the spontaneous alloying mechanism even under the low temperature.[55-57]

The XPS spectra of Au_xPd_y-PVP NCs were measured in order to discuss the charge transfer between two metals. The peaks around Au 4*f* components are shown in Figure 4(A). The humped peaks were contributed to the Au $4f_{7/2}$ (around at 83 eV) and $4f_{5/2}$ (around at 87 eV). All Au_xPd_y-PVP NCs exhibited negative shifts in the both Au 4*f* binding energies compared to that of pure Au foil (84.0 and 88.0 eV).[58] Importantly, increasing the Pd contents induced more shifts in binding energy to the lower energy side (Figure 4(B)). Thus, it is supposed that the charge transfer from Pd to Au atoms was facilitated by increase in Pd contents of Au_xPd_y-PVP NCs. The largest negative shift in Au $4f_{7/2}$ was -1.96 eV in the case of $Au_{20}Pd_{80}$-PVP NCs. The negative shifts of binding energy in the Au $4f_{7/2}$ peak were also reported in the crown-jewel-structured Au_{12}/Pd_{147}-PVP NCs (-1.5 eV),[9] Au_{90}-Ag_{10}-PVP alloy NCs (-1.4 eV),[43] $Au_1@Pt_4$-Rh_{20}-PVP NCs (-0.15 eV),[44] and $Au_{90}Pt_5Ag_5$-PVP NCs (-1.4 eV).[45] The large number of negative sift in Au 4*f* peak supposed that the Au_xPd_y-PVP NCs have a lot of agglutinations between Au and Pd atoms, which increased the opportunity for electron transfer from Pd to Au atoms. While, the XPS peaks in Pd 3*d* were hard to analyzed because of weak intensities and energy overlapping at 335.0 eV corresponding to Pd $3d_{5/2}$ and Au $4d_{5/2}$ (Figure S7).[58] It was reported that the Pd NCs with a diameter less than 2.0 nm have an amorphous structure whereas that with a diameter more than 2.5 nm have crystalline structures.[59] It is indicated that the phase transfer of Pd NCs was found between 2.5 and 4.0 nm. In our case, the average size of Au_xPd_y-PVP NCs were below 2.7 nm. Therefore, the Pd atoms in the Au_xPd_y cluster supposedly composed the amorphous structure of Pd aggregates and/or the less ordered AuPd structure, and which makes the Pd related peaks broadening. From XPS analysis, the electron transfer from Pd to Au was elucidated, however, the correlation between the electron transfer and their catalysis still remains unclear.

To confirm the presence of the electronic negative Au atoms in Au_xPd_y-PVP NCs, Au L_3-edge XANES spectra were also measured for AuPd-PVP/HTs, as shown in Figure 5(A). The white-line (WL) feature in the L_3-edge spectrum is related to the transition of 2*p* electron to unoccupied 5*d* electron states. Though the unperturbed Au atom possesses no holes in 5*d* orbital (electron configuration $[Xe]6s^14f^{14}5d^{10}$), the Au bulk L_3-edge XANES spectra exhibits the WL feature due to the *s*-*p*-*d* hybridization which lead to the small amount of electron transformation from 5*d* to *s*-*p* states.[60-62] The WL features around 11.925 eV in the Au_xPd_y-PVP/HTs indicated lower intensities than Au foil (Figure 5(A)). Therefore, it was supposed that the Au_xPd_y-PVP/HTs contained more 5*d* electrons than Au foil. To further elucidate the differences in the 5*d* electron densities among Au_xPd_y-PVP/HTs, the areas of WL features in Au_xPd_y-PVP/HTs were calculated. Because the width in the WL feature depends on the lifetime of core hole, the dipole-transition matrix element, and the distribution of the density of states of unoccupied *d* band at the Fermi level of the element,[60] the range from 10 eV below the X-ray absorption edge (E_o) to 13 eV above the E_o was applied for calculation.[63,64] Here, $\mu_3 = 107.7\ cm^2 \cdot g^{-1}$ and $\rho = 19.32\ g \cdot cm^{-3}$ are the X-ray absorption cross section at L_3-edge jump and the density of Au, respectively. The areas as a function of Pd contents were plotted with the yield of acetophenone in Figure 5(B). The area of Au L_3-edge XANES spectrum was

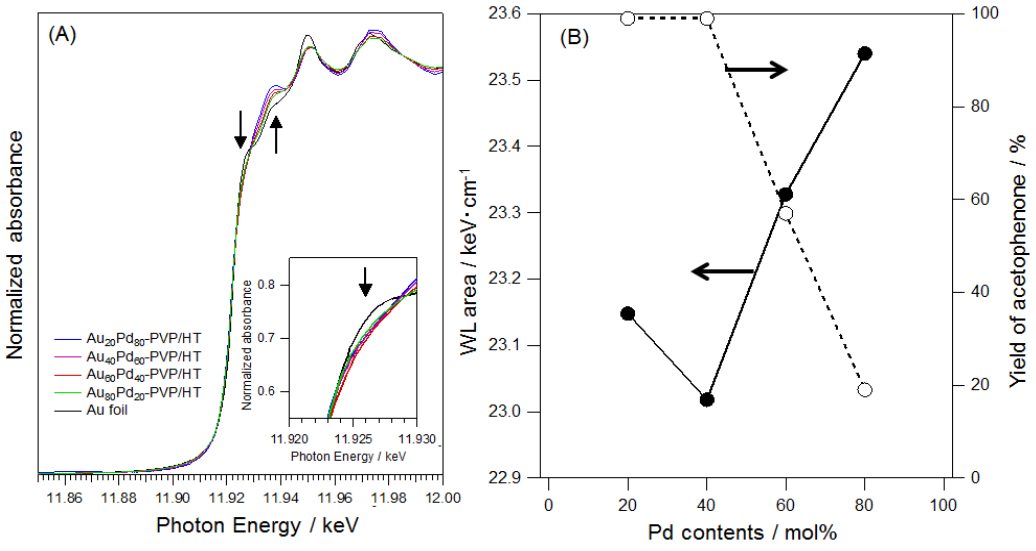

Fig. 5 (A) The changes in Au L_3-edge XANES spectra and (B) Correlations between the area in the range of -10 eV < E_o < 13 eV among Au_xPd_y-PVP/HT catalysts with various Pd contents.

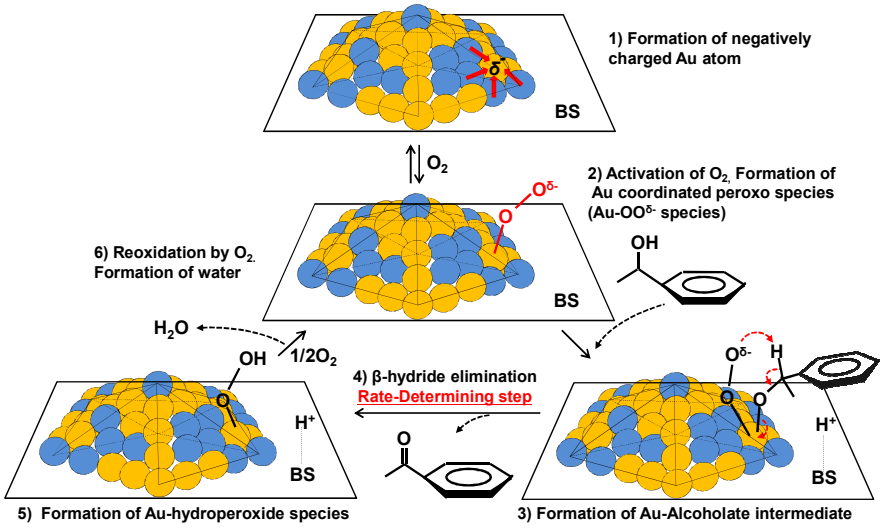

Fig. 6 Proposed reaction mechanism of alcohol oxidation over Au_xPd_y-PVP/HT catalysts.

contributed to the amount of 5*d* holes in Au atoms. In other word, the area decreased with increasing the 5*d* electrons. Therefore, it was clarified that the $Au_{60}Pd_{40}$-PVP/HT possessed the largest number of the 5*d* electron-rich Au atoms among Au_xPd_y-PVP/HTs. Relationships between the areas and yield of acetophenone as a function of Pd contents implied that the electron density of 5*d* states in Au atoms was strongly contributed to the catalytic activity for aerobic oxidation (Figure 5(B)). One other important feature as the increasing of intensities with increased Pd contents around at 11.935 keV was also observed in the Au L_3-edge XANES spectra (Figure 5(A)). It seemed to be an evidence of the homogeneously-mixed AuPd alloy formation because these features were relatively sensitive to the interatomic redistribution of charge when Au and Pd atoms come closer together or further apart in AuPd NPs.[65-68]

We proposed the catalytic cycle for alcohol oxidation over the Au_xPd_y-PVP/HT catalysts in Figure 6, which proceeds *via* alkoxide intermediates and radical-like peroxo-species. Firstly, an O_2 molecule adsorbed onto the negatively charged Au site on Au_xPd_y NCs, then the adsorbed molecular O_2 is dissociated through the electron donation from Au 5*d* to the antibonding $2\pi^*$ orbital of O_2 (AuO^{2-} peroxo- and/or AuO_2^{2-} superoxo-species formation). The adsorbed molecular (*ex.* CO and O_2) activation on anionic and/or neutral Au clusters was also suggested in the literatures based on the experiment and theoretical studies.[69-73] This proposed step agrees well with Au-PVP NC catalysts for aerobic oxidation of alcohol.[74] Secondary, an alcohol molecular is dissociatively adsorbed on the Au and/or Pd affording the [metal-alkoxide]$^-$ (oxidative addition). The HT basicity promotes this process owing to abstracting of proton from alcohol involving $[H\text{-}HT]^+$ formation. Third, the H atom on the α-carbon of the adsorbed alkoxide is transformed to the Au-peroxo- (and/or superoxo-) species (β–hydrogen elimination), then the corresponding

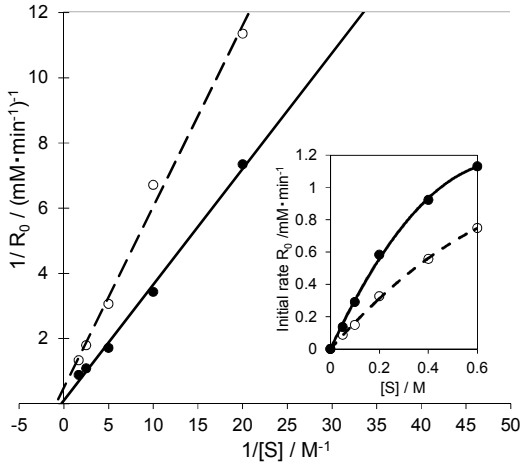

Fig. 7 Lineweaver-Burk plot and Michaelis-menten kinetics in the aerobic oxidation of 1-phenyl ethanol over the $Au_{60}Pd_{40}$-PVP/HT (solid line) and bare Au_{100}/HT (dash line) catalysts. Reaction conditions : 1-phenylethanol (0.25-3 mmol), catalyst (10 mg), toluene 5 mL, 313 K, 5 min, O_2 flow (20 mL•min^{-1}).

carbonyl compound and Au-hydroperoxide species were formed.[75] Finally, another O_2 attacked and removed the hydroperoxide species from the Au surface with the formation of H_2O, thereby, the catalytic cycle was completed.[76] The Au_xPd_y NCs seems to have key factors in this step since the β–hydrogen elimination is considered as the rate-determination step in the alcohol oxidation *via* alkoxide formation in the previous reports.[14,18]

According to the these reaction mechanism, both the $[RCH(O)CH_3\text{-}(AuPd)\text{-}OO^{\delta-}]$ type of Michaelis complex and Michaels-Menten-type kinetics [Eq.(1)] were assumed in the 1-phenylethanol oxidation over Au_xPd_y-PVP/HT catalyst. Because the Lineweaver-Burk plots in the oxidation of

$$(AuPd)^{\delta-} + RCH(OH)CH_3 + O_2 \underset{k_{-1}}{\overset{k_1}{\rightleftharpoons}} [RCH(O)CH_3\text{-}(AuPd)\text{-}OO^{\delta-}] \xrightarrow{k_2} (AuPd)\text{-}OOH + RCOCH_3 \quad \text{Eq. (1)}$$

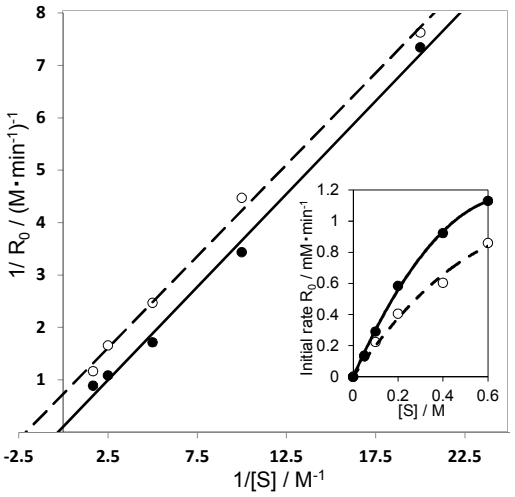

Fig. 8 Lineweaver-Burk plot and Michaelis-menten kinetics in the aerobic oxidation of 1-phenyl ethanol over the $Au_{60}Pd_{40}$-PVP/HT catalyst in the presence (solid line) and absence (dash line) of TEMPO radical scavenger. Reaction conditions : 1-phenylethanol (0.25-3 mmol), catalyst (10 mg), TEMPO (0.0032 mmol), toluene 5 mL, 313 K, 5 min, O_2 flow (20 mL•min^{-1}).

1-phenyl ethanol over the $Au_{60}Pd_{40}$-PVP/HT catalyst showed good liner collation between the inverse of initial rate ($1/R_o$) and the inverse of substrate concentration (1/substrate) (Figure 7(A)), the oxidation of 1-phenylethanol follows the Michaels-Menten-type kinetics. This is because the primary alcohol oxidation over the bare Au supported catalyst also Michaels-Menten-type kinetics [Eq.(1)]. The alcohol oxidation over bare Au_{100}/HT catalyst also agrees well with the mechanism *via* the similar [RCH_2O-Au] intermediate.[14,37]

In the case of the $Au_{60}Pd_{40}$-PVP/HT catalyst, K_M and k_2 were calculated to be 3228 mM and 0.152 mM s^{-1}, respectively, whereas over the bare Au_{100}/HT catalyst, they were 1112 mM and 0.033 mM s^{-1}. It was indicated that the rate of β–hydrogen elimination was drastically facilitated in the bimetallic AuPd-PVP/HT catalyst than that in the monometallic Au_{100}/HT catalyst. To further investigate the reaction mechanism, the results of Lineweaver-Burk plot and Michaelis-Menten kinetics in the aerobic oxidation of 1-phenylethanol over the $Au_{60}Pd_{40}$-PVP/HT were compared in the presence and absence of TEMPO as a radical scavenger (Figure 8). In the presence of TEMPO, the both K_M and k_2 were decreased to be 475 mM and 0.023 mM s^{-1}, respectively, whereas the slopes in the Lineweaver-Burk plot (K_m/V_{max}) were similar irrespective of TEMPO. Therefore, TEMPO affected onto the reaction pathway by the uncompetitive inhibition mechanism; *i.e.* TEMPO is not combined with the active site but intermediate species. Since TEMPO cannot combine the alkoxide intermediate,[17,49] the prospective radical-like peroxo- species were protected by TEMPO and which makes the reaction slower. These results suggested that the remarkable activity of Au_xPd_y-PVP/HT catalysts for aerobic oxidation of alcohols might be originated from the negatively charged Au (5*d* states) generating the peroxo- and/or superoxo- species which strongly enhances the reaction rate in the β–hydrogen elimination of the alkoxide intermediates.

Conclusions

The effect of intermetallic charge transfer in bimetallic nanoparticles was examined by using Au_xPd_y-PVP NCs supported onto HT catalysts (Au_xPd_y-PVP/HT) with narrow particle size distributions. The Pd contents in the Au_xPd_y-PVP/HT strongly influenced the activities for the aerobic oxidation of alcohols. The XPS analysis suggested the electron transfer from Pd to Au atoms was facilitated by increase in Pd contents of Au_xPd_y-PVP NCs. The close correlations between the electron density in the Au 5*d* state and reaction activity was obtained by the Au L_3-edge XANES analysis of the Au_xPd_y-PVP/HTs. Moreover, the Michaels-Menten-type kinetic studies clearly indicated that the electron rich Au 5*d* states strongly accelerated the rate-determination step in the alcohol oxidation. These findings pointed out that design of electron transfer using heterometallic catalyst may form guiding principle for further endeavors in the field of bimetallic nanocatalysis, and atomic-scale design of nanoparticles with remarkable catalysis.

Notes and references

[a] *School of Materials Science and ‡Center for Nano Materials and Technology, Japan Advanced Institute of Science and Technology, 1-1 Asahidai, Nomi, Ishikawa 923-1292, Japan, Fax: +81-761-51-1613, Tel: Fax: +81-761-51-1149, E-mail: ebitani@jaist.ac.jp*
[b] *Center for Nano Materials and Technology, Japan Advanced Institute of Science and Technology, 1-1 Asahidai, Nomi, Ishikawa 923-1292, Japan*

† Electronic Supplementary Information (ESI) available: [UV-vis, XPS, STEM-EDS, and results of alcohol oxidations]. See DOI: 10.1039/b000000x/

‡ Abbreviations; PVP, poly(*N*-vinyl-2-pyrrolidone); PVA, poly(vinyl alcohol); X@Y, X-core Y-shell (X, Y; element).

1 N. Toshima and T. Yonezawa, *New J. Chem.*, 1998, **22**, 1179-1201.
2 M. Haruta, T. Kobayashi, H. Sano and N. Yamada, *Chem. Lett.*, 1987, **16**, 405-408.
3 M. Haruta, N. Yamada, T. Kobayashi and S. Iijima, *J. Catal.*, 1989, **115**, 301-309.
4 A. Stephen, K. Hashmi and G. J. Hutchings, *Angew. Chem., Int. Ed.*, 2006, **45**, 7896-7936.
5 G. J. Hutchings, *Gold Bull.*, 1996, **29**, 123-130.
6 M. Haruta, *Nature*, 2005, **437**, 1098-1099.
7 T. Ishida and M. Haruta, *Angew. Chem., Int. Ed.*, 2007, **46**, 7154-7156.
8 P. Schwerdtfeger, *Angew. Chem., Int. Ed.*, 2003, *42*, 1892-1895.
9 H. Zhang, T. Watanabe, M. Okumura, M. Haruta and N. Toshima, *Nature Mater.*, 2012, **11**, 49-52.
10 D. Xu, X. Liu, H. Yang, Q. Liu, J. Zhang, J. Fang, S. Zou and K. Sun, *Angew. Chem., Int. Ed.*, 2009, **48**, 4217-4221.
11 T. Ebashi, Y. Ishida, Y. Nakagawa, S. Ito, T. Kubota and K. Tomishige, *J. Phys. Chem. C*, 2010, **114**, 6518-6528.
12 A. Abad, P. Concepcion, A. Corma and H. Garcia, *Angew. Chem., Int. Ed.*, 2005, **44**, 4066-4069.
13 A. Abad, C. Almela, A. Corma and H. Garcia, *Tetrahedron*, 2006, **62**, 6666-6672.
14 A. Abad, A. Corma and H. Garcia, *Chem. Eur. J.*, 2008, **14**, 212-222.
15 K. Ebitani, K. Motokura, T. Mizugaki and K. Kaneda, *Angew. Chem., Int. Ed.*, 2005, **44**, 3423-3426.
16 K. Yamaguchi and N. Mizuno, *Angew. Chem., In. Ed.*, 2002, **41**, 4538-4542.
17 K. Yamaguchi and N. Mizuno, *Chem. Eur. J.*, 2003, **9**, 4353-4361.
18 K. Yamaguchi, K. Mori, T. Mizugaki, K. Ebitani and K. Kaneda, *J. Am. Chem. Soc.*, 2000, **122**, 7144-7145.

19 D. I. Enache, J. K. Edwards, P. Landon, B. Solsona-Espriu, A. F. Carley, A. A. Herzing, M. Watanabe, C. J. Kiely, D. W. Knight and G. J. Hutchings, *Science*, 2006, **311**, 362-365.

20 G. L. Brett, Q. He, C. Hammond, P. J. Miedziak, N. Dimitratos, M. Sankar, A. A. Herzing, M. Conte, J. A. Lopez-Sanchez, C. J. Kiely, D. W. Knight, S. H. Tayor and G. Hutchings, *Angew. Chem., Int. Ed.*, 2011, **50**, 10136-10139.

21 N. Dimitratos, J. A. Lopez-Sanchez, S. Meenakshisub-daram, J. M. Anthonykutty, G. Brett, A. F. Carley, S. H. Taylor, D. W. Knight and G. J. Hutchings, *Green Chem.*, 2009, **11**, 1209-1216.

22 A. Villa, C. Campione and L. Prati, Catal. Lett., 2007, 115, 133-136.

23 Y. Shi, H. Yang, X. Zhao, T. Cao, J. Chen, W. Zhu, Y. Yu and Z. Hou, *Catal. Commun.*, 2012, **18**, 142-146.

24 K. Kaizuka, H. Miyamura and S. Kobayashi, *J. Am. Chem. Soc*., 2010, **132**, 15096-15098.

25 N. Toshima, M. Haruta, Y. Yamazaki and K. Asakura, *J. Phys. Chem.*, 1992, **96**, 9927-9933.

26 H. Liu, G. Mao and S. Meng, *J. Mol. Catal.*, 1992, **74**, 275-284.

27 J. K. Edwards, B. Solsona, N. E. Ntainjua A. F. Carley, A. A. Herzing, C. J. Kiely and G. J. Hutchings, *Science*, 2009, **323**, 1037-1041.

28 P. Landon, P. J. Collier, A. J. Papworth, C. J. Kielyc and G. J. Hutchings, *Chem. Commun.*, 2002, 2058-2059.

29 P. Landon, P. J. Collier, A. F. Carley, D. Chadwick, A. J. Papworth, A. Burrows, C. J. Kiey and G. J. Hutchings, *Phys. Chem. Chem. Phys.*, 2003, **5**, 1917-1923.

30 M. Chen, D. Kumar, C.-W. Yi and D. W. Goodman, *Science*, 2005, **310**, 291-293.

31 J. H. Shim, J. Kim, C. Lee and Y. Lee, *Chem. Mater.*, 2011, **23**, 4694-4700.

32 M. Nie, P. K. Shen and Z. Wei, *J. Power Sour.*, 2007, **167**, 69-73.

33 T. Mitsudome, A. Noujima, Y. Mikami, T. Mizugaki, K. Jitsukawa and K. Kaneda, *Angew. Chem., Int. Ed.*, 2010, **49**, 5545-5548.

34 T. Mitsudome, Y. Mikami, M. Matoba, T. Mizugaki, K. Jitsukawa and K. Kaneda, *Angew. Chem., Int. Ed.*, 2012, **51**, 136-139.

35 T. Mitsudome, A. Noujima, T. Mizugaki, K. Jitsukawa and K. Kaneda, *Green Chem.*, 2009, **11**, 793-797.

36 T. Mitsudome, A. Noujima, T. Mizugaki, K. Jitsukawa and K. Kaneda, *Adv. Synth. Catal.*, 2009, **351**, 1890-1896.

37 N. K. Gupta, S. Nishimura, A. Takagaki and K. Ebitani, *Green Chem.*, 2011, **13**, 824-827.

38 A. Takagaki, M. Takahashi, S. Nishimura and K. Ebitani, *ACS Catal.,* 2011, **1**, 1562-1565.

39 A. Tsuji, K. T. V. Rao, S. Nishimura, A. Takagaki and K. Ebitani, *ChemSusChem*, 2011, **4**, 542-548.

40 N. Toshima, *Pure Appl. Cham.*, 2000, **72**, 317-325.

41 N. Toshima, M. Harada, T. Yonezawa, K. Kushihashi and K. Asakura, *J. Phys. Chem.*, 1991, **95**, 7448-7453.

42 H. Hakkine, S. Abbet, A. Sanchez, U. Heiz and U. Landman, *Angew. Chem., Int. Ed.*, 2003, **42**, 1297-1300.

43 N. K. Chaki, H. Tsunoyama, Y. Negishi, H. Sakurai and T. Tsukuda, *J. Phys. Chem. C*, 2007, **111**, 4885-4888.

44 N. Toshima, R. Ito, T. Matsushita and Y. Shiraishi, *Catal. Today*, 2007, **122**, 239-244.

45 H. Zhang, M. Okumura and N. Toshima, *J. Phys. Chem. C*, 2011, **115**, 14883-14891.

46 D. Ferrer, A. Torres-Castro, X. Gao, S. Sepulveda-Guzman, U. Ortiz-Mendez and M. Jose-Yacaman, *Nano Lett.*, 2007, **7**, 1701-1705.

47 The TON and TOF were estimated as > 682,300 and 119,260 h^{-1}, respectively, assuming only Au atoms could act as active sites in 0.2 g of $Au_{60}Pd_{40}$-PVP/HT catalyst.

48 In the standard condition for comparing the catalytic activities among heterogeneous catalysts (40 mmol scale of 1-phenylethanol), the TON exhibited at up to 207,000 at 423 K for 24 h (> 99 % yield and selectivity).

49 K. Mori T. Hara, T. Mizugaki, K. Ebitani and K. Kaneda, J. Am. Chem. Soc., 2004, 126, 10657-10666.

50 H. Tomioka, K. Takai, K. Oshima and H. Nozaki, *Tetrahedron Lett.*, 1981, **22**, 1605-1608.

51 S. Kanemoto, S. Matsubara, K. Takai, K. Oshima, K. Utimoto and H. Nozaki, *Bull. Chem. Soc. Jpn.*, 1988, **61**, 3607-3612.

52 A. Hanyu, E. Takezawa, S. Sakaguchi and Y. Ishii, Tetraheron Lett. 1998, 39, 5557-5560.

53 L. P. Hammet, *J. Am. Chem. Soc.*, 1937, **59**, 96-103.

54 S. Link and M. A. El-Sayed, *J. Phys. Chem. B*, 1999, **103**, 4212-4217.

55 H. Yoshida, H. Mori, M. Komatsu and K. Takeda, *Appl. Phys. Lett.*, 1992, **61**, 2173-2174.

56 H. Yoshida and H. Mori, *Phys. Rev. Lett.*, 1992, **69**, 3747-3750.

57 Y. Shimizu, K. S. Ikeda and S. Sawada, *Phys. Rev. B*, 2001, **64**, 075412.

58 J. F. Moulder, W. F. Stickel, P. E. Sobol and K. D. Bomben, Handbook of X-ray Photoelectron Spectroscopy (Ed.: J. Chastain), Perkin-Elmer Co., Minnesota, 1992.

59 J. S. Bradley, E. W. Hill, S. Behal, C. Klein, B. Chaudret and A. Duteil, *Chem. Mater.*, 1992, **4**, 1234-1239.

60 T. K. Sham, *Phys. Rev. B*, 1985, **31**, 1888-1902.

61 L. F. Mattheiss and R. E. Dietz, *Phys. Rev. B*, 1980, **22**, 1663-1676.

62 V. V. Nemoshkalenko, V. N. Antonov, W. John, H. Wonn and P. Ziesche, *Phys. Status Solidi B*, 1982, **111**, 11-52.

63 A. N. Mansour, J. W. Cook and D. E. Sayers, *Phys. Chem.*, 1984, **88**, 2330-2334.

64 S. Nishimura, A. T. N. Dao, D. Mott, K. Ebitani and S. Maenosno, *J. Phys. Chem. C*, 2012, **116**, 4511-4516.

65 M. O. Pedersen, S. Helveg, A. Ruban, I. Stensgaard, E. Laegsgaard, J. K. Norskov and F. Besenbacher, *Sur. Sci.*, 1999, **426**, 395-409.

66 S. N. Reifsnyder and H. H. Lamb, *J. Phys. Chem. B*, 1999, **103**, 321-329.

67 P. Dash, T. Bond, C. Fowler, W. Hou, N. Coombs and R. W. J. Scott, *J. Phys. Chem. C*, 2009, **113**, 12719-12730.

68 T. Balcha, J. R. Strobl, C. Fowler, P. Dash and R. W. J. Scott, *ACS Catal.*, 2011, **1**, 425-436.

69 B. Yoon, H. Hakkinen, U. Landman, A. S. Worz, J.-M. Antonietti, S. Abbet, K. Judai and U. Heiz, *Science*, 2005, **307**, 403-407.

70 L. D. Socaciu, J. Hagen, T. M. Bernhardt, L. Woste, U. Hwiz, H. Hakkinen and U. Landman, *J. Am. Soc.*, 2003, **125**, 10437-10445.

71 D. Stolcic, M. Fischer, G. Gantefor, Y. D. Kim, Q. Sun and P. Jena, *J. Am. Chem. Soc.*, 2003, **125**, 2848-2849.

72 B. Yoon, H.; Hakkinen and U. Landman, *J. Phys. Chem. A*, 2003, **107**, 4066-4071.

73 B. E. Salisury, W. T. Wallace and R. L. Whetten, *Chem. Phys.*, 2000, **262**, 131-141.

74 H. Tsunoyama, N. Ichikuni, H. Sakurai and T. Tuskuda, *J. Am. Chem. Soc.*, 2009, **131**, 7086-7093.

75 The electron transfer from the alkoxides to Au and/or Pd occurred during this step. The formation of Au-hydroperoxide species *via* β–hydride elimination through short life-timed hydride was also considerable though the presence of peroxo-species on the active sites might limit its formation.

76 The H_2O_2 formation in the reaction medium could not be detected by an oxidation-reduction titration.